Protocells Featuring Membrane-Bound and Dynamic Membraneless Organelles

Clémence Schvartzman, Emmanuel Ibarboure, Anouk Martin, Elisabeth Garanger, Angela Mutschler, Sébastien Lecommandoux*

Univ. Bordeaux, CNRS, Bordeaux INP, LCPO, UMR 5629, F-33600 Pessac, France

ABSTRACT

Living cells, especially eukaryotic ones, use multi-compartmentalization to regulate intra- and extracellular activities, featuring membrane-bound and membraneless organelles. These structures govern numerous biological and chemical processes spatially and temporally. Synthetic cell models, primarily utilizing lipidic and polymeric vesicles, have been developed to carry out cascade reactions within their compartments. However, these reconstructions often segregate membrane-bound and membraneless organelles, neglecting their collaborative role in cellular regulation. To address this, we propose a structural design incorporating microfluidic-produced liposomes housing synthetic membrane-bound organelles made from self-assembled poly(ethylene glycol)-*block*-poly(trimethylene carbonate) nanovesicles and synthetic membraneless organelles formed via temperature-sensitive elastin-like polypeptides (ELPs) phase separation. This architecture mirrors natural cellular organization, facilitating detailed examination of interactions for a comprehensive understanding of cellular dynamics.

KEYWORDS: artificial cells, synthetic organelles, elastin-like polypeptides, microfluidics, liquid-liquid phase separation, self-assembly

INTRODUCTION

The fundamental building block of living organisms is the cell, the universal biological base of all living entities. This micrometric mass of cytoplasm composed of more than thousands of biological and chemical molecules and structured with a cytoplasmic membrane has fascinated scientists for its highly complex and multi-compartmentalized structure[1]. Each of these sub-compartments is an organized and specialized functional unit and this specific feature allows to the global system to control spatiotemporally biological events specifically and individually, without any interference[2–4]. These sub-compartments also possess the properties to encapsulate, protect, and control the release of bio(macro)molecules through selective transport processes, crucial for the development and the survival of the cell. These sub-compartments, also referred as organelles, play a vital role in coordinating numerous processes within eukaryotic cells, facilitating efficient segregation of biochemical activities. This multicompartmental cellular arrangement enhances effectiveness by ensuring distinct processes occur with precision. These cellular compartments are integral to functions like cellular recognition, immune responses, neuromuscular transmission, and overall cellular organization within tissues and organs. As a result, synthetic multicompartmentalized structures have been developed[5] using artificial vesicle systems like polymersomes, liposomes, and coacervates[6]. Therefore, two distinct type of organelles can be described, the first and more popular one being named membrane-bound organelle,[7–9] such as

lysosome, that is a self-assembled structure containing a subcellular aqueous environment surrounded by a unilamellar lipid membrane. The second organelle, defined as membraneless organelle[10,11], such as the nucleoli and processing bodies (P-bodies), is devoid of any lipid boundary and became the focus of research in cell biology this last decade, as Brangwynne and coworkers have enlightened their unique role and function within eukaryotic cells[12]. As a matter of fact, these sub-compartments can be formed through liquid-liquid phase separation (LLPS) of ribonucleic acid (RNA) and intrinsically disordered proteins (IDP) and this formation of coacervates is mainly driven by environmental variations (pH, temperature, osmotic stress, *etc*.)[13–15]. The creation of protocells that possess the ability of generating numerous chemical and biological reactions has been one of the challenges of the last decades since the first design of artificial cell in 1957[16,17] and nowadays, the bottom-up construction of a synthetic cell using non-living materials represents an important challenge. Because of their structural similarity to cell membranes, liposomes[18–25] and polymersomes[26–30] have been widely used as synthetic cell-like compartments, as well as proteinosomes,[31–33] (inorganic) colloidosomes,[34] and membrane-free coacervate microdroplets[35–37], commonly prepared using microfluidic systems[20,38], film-rehydration[39], or emulsion-centrifugation[7] techniques. To further increase the complexity of these prototypes, multi-compartmentalized architectures were developed by encapsulating sub-compartments within these larger ones. As an example, membrane-bound encapsulated systems were designed by encapsulating liposomes-in-liposome[40–44], liposomes in layer-by-layer capsule[45], polymersomes-in-polymersome[46], capsosomes[47–49], and liposomes-in-polymersome[9]. Concerning the design of the second type of artificial organelle, membraneless systems were designed by encapsulating coacervates-in-vesicle[38,50–53], coacervates-in-Aqueous Two-Phase System (ATPS)[54,55], coacervates-in-droplet[56–59], and coacervates-in-coacervate[60]. Chemical and

biochemical components are usually integrated within these systems, capable of accomplishing increasingly intricate functions[5,61] following an external stimulus, such as light[59], pH[51], temperature[56,57] and osmolarity[62] variations. A variety of cellular processes like cell division[63] and self-sustainability[64] can be achieved, the latter being the next important challenge of this field. Despite significant progress in constructing complex artificial cells, it has been observed that bottom-up constructions systematically separate the two main types of organelles, which does not accurately represent the structural and biological function of a living cell. However, Zhao *et al.* recently reported how these condensates intimately interact in eukaryotic cells and regulate their various activities[65].

In this study, our goal was to construct a multicompartmental artificial cell by co-encapsulating synthetic organelles, that mimic both types of natural organelles, within a cytoplasm-like core. We thus incorporated poly(ethylene glycol)-*block*-poly(trimethylene carbonate) nanovesicles tagged with a fluorescent dye Cyanine 5.5 (PEG$_{22}$-*b*-PTMC$_{51}$-Cy5.5), representing membrane-bound organelles, and temperature-sensitive Elastin-like Polypeptides (ELPs), representing membraneless organelles, into a PEG crowded lumen. ELPs are intrinsically disordered protein (IDP) models that can undergo phase separation and form coacervates in response to temperature and/or concentration changes. We demonstrated the coexistence and functional efficacy of synthetic organelles within the cell-like chassis, each carrying out its designated tasks. We believe that our unique prototype combines multiple vital cell components and has the potential to pave the way for developing advanced artificial cell models that emulate the behaviors of living cells.

Experimental (Materials and Methods)

Materials. Poly(ethylene glycol) (PEG, 6 kDa) polymer was purchased from Alfa Aesar. Poly(vinyl alcohol) (PVA, 13-23 kDa, 87-89% hydrolyzed) polymer was obtained from Sigma-Aldrich. L-α-phosphatidylcholine (Egg PC, 25 mg.ml^{-1} in chloroform) was bought from Avanti Polar Lipids. Pluronic$^{®}$ F-68 was obtained from Gibco. Cyanine 5.5-NH$_2$ was obtained from Lumiprobe. All compounds were used without further purification. The following solvents were purchased from Sigma-Aldrich and used without further purification: chloroform (anhydrous, 99%), hexane (anhydrous, 95%), dimethyl sulfoxide (DMSO, 99.9%). Acetone was purchased from VWR. Phosphate-Buffer Saline (PBS) 10X was purchased from Euromedex. 10X refers to the concentration of the solution that needs to be diluted 10 times. 10X solution is composed of KH$_2$PO$_4$: 10.6 mM, Na$_2$HPO$_4$, 2H$_2$O: 30.0 mM, NaCl: 1.54 M. Water with a resistivity of 18.2 MΩ.cm^{-1} was prepared using a Millipore Milli-Q system. PEG$_{22}$-*b*-PTMC$_{51}$ was synthetized by ring-opening polymerization of TMC using MeO-PEG$_{22}$-OH as macroinitiator (f$_{PEG}$=16.1%, Đ=1.04, Mn=6,200 g.mol^{-1}). PEG$_{22}$-*b*-PTMC$_{51}$-Cy5.5 was obtained from post-functionalization of PEG$_{22}$-*b*-PTMC$_{51}$-COOH with Cyanine 5.5-NH$_2$.

Bioproduction, isolation and purification of ELP[M$_1$V$_3$-80]. ELPs are repeat units of a Val-Pro-Gly-Xaa-Gly (VPGXG) pentapeptide sequence, produced recombinantly in *Escherichia coli* (*E. coli*) bacteria[66], and serve as IDP models. Methionine-containing temperature-sensitive ELPs were used and named ELP[M$_1$V$_3$-80], with a primary structure of 80 repeat units of a pentapeptide presenting Val/Met as guest residues in a 3:1 ratio. ELP[M$_1$V$_3$-80] was produced by recombinant DNA and protein engineering techniques in *E. coli* and isolated using previously reported procedures[67, 68,69]. The notation of this ELP is shortened to ELP M80 in the following.

Self-assembly of PEG$_{22}$-b-PTMC$_{51}$-Cy5.5. Dolomite microfluidics™ system was used to induce microfluidic assisted self-assembly of PEG$_{22}$-*b*-PTMC$_{51}$-Cy5.5. The system is composed of two

Mitos pressure pumps equipped with flowmeters allowing flows to run in a micromixer chip of 12 mixing stages and connection is ensured by ethylene propylene tubing. The pump containing the organic solution was connected to first and third inputs using a T-connector, the aqueous solvent pump being connected directly to second input of the chip. Briefly filtered 10 mg.mL^{-1} of copolymer solution in DMSO (with 98 %wt PEG$_{22}$-*b*-PTMC$_{51}$+ 2 %wt PEG$_{22}$-*b*-PTMC$_{51}$-Cy5.5) and filtered PBS were used for the formulation of polymersomes with a total flow rate of 1,000 µL.min^{-1} and a ratio between organic and aqueous solvent of 20:80 vol%. After formulation by microfluidic, dynamic light scattering (DLS) measurements were performed on Nano-ZS-90 instrument (Malvern) at a 90° angle, running 5 measurements of 8 runs of 8 s. D_H and PDI were calculated from autocorrelation functions using cumulant methods and were averaged. The organic solvent was removed by dialysis against PBS buffer, with 3 baths of 2 L each using 25 kDa pre-wetted dialysis membrane tubing. DLS 90° were done the same way as previously reported after samples were filtrated with a 0.45 µm cellulose acetate syringe filter.

Microfluidic design for formulation of liposomes. The protocol to design the microfluidics device for the formulation of the liposomes can be found according to this reference[62]. Briefly, two cylindrical capillaries of inner diameter 580 µm and outer dimension 1 mm (World precision instruments, 1B100-4) were tapered by a micropipette puller (Sutter instrument, P-97) followed by polishing the orifices with sand papers into 60 µm and 120 µm, respectively. The capillary with the smaller orifice was treated hydrophobically with sigmacote, while the surface of the larger capillary was rendered hydrophilic with APTES and used as a collection channel. A square capillary (VitroCom, 2956C1) was used to nest both cylindrical capillaries that were inserted in opposite directions. Lastly, dispensing needles used as inlets of fluids were connected at the junctions between capillaries by using a transparent 5 min Epoxy (Devcon). The devices were

connected to high-precision syringe pumps (Chemyx, Fusion 100) *via* poly(ethylene) tubing (Scientific Commodities Inc., BB31695-PE/4) to ensure reproducible and stable flows.

Formation of double emulsion microdroplets. For the encapsulation of the two types of organelles, the formulation of water-in-oil-in-water (W/O/W) double-emulsion microdroplets was performed (Figure 1). Briefly, an aqueous PEG phase, concentrated at 8 wt% and containing 1 mg.mL^{-1} of ELP M80, and 0.20 mg.mL^{-1} of Cy5.5-tagged PEG$_{22}$-*b*-PTMC$_{51}$ nanovesicles was flowed in the injection capillary as the innermost solution. This 8 wt% concentration was chosen to mimic the cell crowding environment, as previously reported[62,63]. An organic mix of chloroform and hexane (36:64 vol%) containing 5 mg.mL^{-1} of Egg PC was used as the middle phase and was injected through the interstices between the injection and square capillaries. The continuous phase of 10 wt% PVA with 0.2% F-68 was pumped through the interstices between the collection and square capillaries. Typical flow rates were set to 500, 1000 and 8000 µL.h^{-1} for inner, middle and outer phases, respectively. These three phases produced double-emulsion microdroplets at the junction, which then flowed along the collection capillary and were collected and sealed with a cover slip in a cavity glass slide (BRAND®).

Confocal microscopy imaging. Microdroplets were collected on a glass slide with a single cavity and sealed using a coverslip for the dewetting process to take place. 10 µL of vesicles were then injected into an imaging chamber (Ibidi GmbH). Images and videos were acquired by a confocal laser scanning microscopy (Leica, SP5 AOBS) through an HCX PL APO 10× dry objective. To assess the spatial distribution of PEG$_{22}$-*b*-PTMC$_{51}$-Cy5.5 nanovesicles inside the partially dewetted microdroplets, a helium-neon diode laser ($\lambda_{Excitation}$ = 633 nm) was used to generate the fluorescence of the Cyanine 5.5 at $\lambda_{Emission}$ = 650-730 nm. To observe and monitor the assembly

of membraneless organelles, ramp temperatures were performed from 10 to 25°C under the bright field mode.

Determination of the transition temperature (T_{cp}) of ELP M80 solutions at different *concentrations by dynamic light scattering (DLS).* To determine the cloud point temperatures (T_{cp}), solutions of 0.25; 1; 2; and 3 mg.mL^{-1} of ELP M80 in a 8 wt% PEG solution were prepared and DLS measurements were performed on Nano-SZ-173 instrument (Malvern) at a constant position in the cuvette (constant scattering volume). The derived count rate (DCR) was defined as the mean scattered intensity normalized by the attenuation factor. The DCR was plotted against temperature and the T_{cp} is defined as the temperature corresponding to the point where the DCR starts increasing on the plot. Temperature ramps were typically performed from 5 to 50 °C for all conditions.

RESULTS AND DISCUSSION

Formation of a cell-like chassis and assembly of synthetic membraneless organelles.

Liposomes are frequently utilized to design synthetic cell-like compartments due to their similarity to cellular membranes in terms of bilayer structure and composition. For that purpose, the self-assembly of L-α-phosphatidylcholine lipids was performed to form the membrane of micron-size unilamellar liposomes, while the external phase was composed of a 0.2% Pluronic F-68 surfactant, that was added to a continuous aqueous phase of 10 wt% poly(vinyl alcohol) (PVA). Therefore, a thick-shell microfluidic system was used to generate a W/O/W double emulsion (Figure 1). By using this technique, partially dewetted liposomes were produced, as described in our prior research[55,62], which we use as an artificial cell-like chassis.
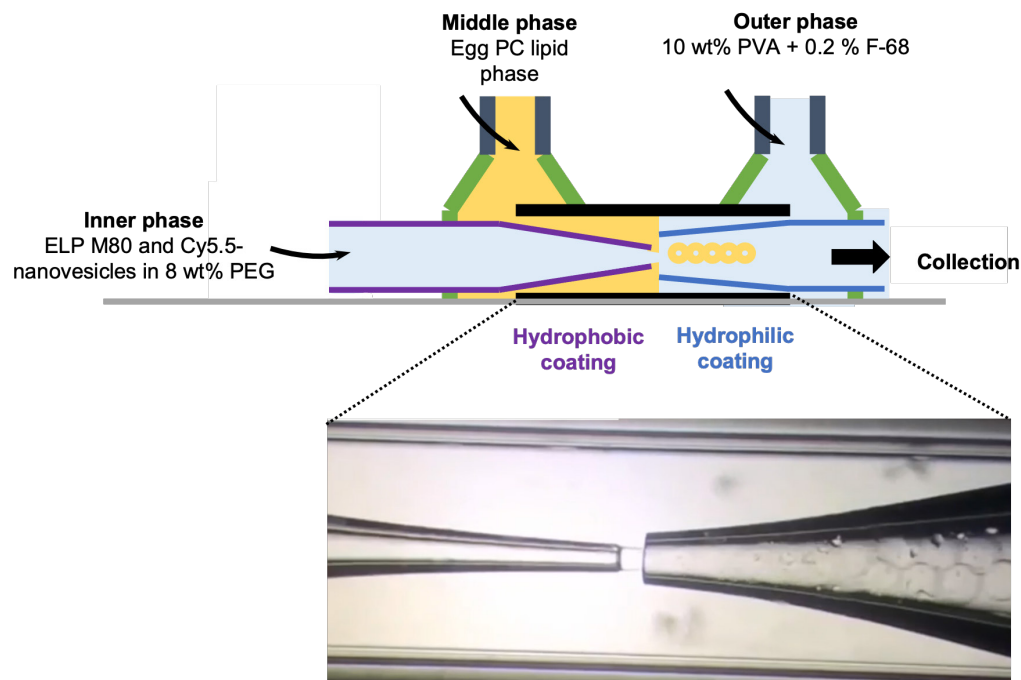
Figure 1. *Schematic representation of a W/O/W double emulsion production using a glass capillary-based microfluidic device.*

Once liposomes were successfully formulated, ELPs were incorporated into the formulation to mimic the synthetic membraneless organelles. It is well-known that ELPs exhibit a lower critical solubility temperature (LCST) phase behavior in aqueous solution, and below their cloud point temperature (T_{cp}), ELPs chains are soluble in water and present as random coil chains (Figure 2a). The T_{cp} can be tuned by varying the nature of amino acid residues of the pentapeptide sequence, in particular at the Xaa position, the number of repeat sequences, and the ELP concentration. Above their T_{cp}, they dehydrate and form ELP-rich coacervates (Figure 2b)[66,70]. The variation of temperature was thus conducted to our liposomes embedded ELPs to trigger the assembly the synthetic membraneless organelles within the crowded lumen. To study this capacity of ELP M80 to undergo Liquid-Liquid Phase Separation (LLPS) and assemble into membraneless organelles within partially dewetted liposomes, several ELP M80 concentrations were

encapsulated in a 8 wt% PEG solution, mimicking the macromolecular crowded environment of a cell.[71] The T_{cp} of 0.25; 1; 2 and 3 mg mL^{-1} of ELP M80 was determined by DLS, each exhibiting a T_{cp} of 21; 18; 15 and 7 °C respectively (Figure 2c). It is noteworthy that the T_{cp} is inversely proportional to concentration, as expected and early demonstrated from Urry[70], consistently illustrated in Figure 2d.

Each of these ELP M80 solutions was then encapsulated individually within the partially dewetted liposomes, and their phase separation was observed. Concerning the impact of the membraneless organelles formation, a higher concentration of the proteins tends to form organelles with a larger size and more contrasted under exposition to the bright light of the microscope; as illustrated in Figure 2g and 2h. Nevertheless, the decrease in T_{cp} in relation to the concentration of the ELPs hindered the selection of these formulations. On the contrary, a concentration of 0.25 mg.mL^{-1} of ELPs was not enough to distinctly observe the phase separation of the ELP M80 within the liposomes (Figure 2e). According to these observations, the solution concentrated at 1 mg.mL^{-1} of ELPs (Figure 2f) was a good compromise as the artificial membraneless organelles were still quite distinct within the lumen under the confocal microscope, with a high enough T_{cp} to experimentally control the phase separation of the ELP M80. Temperature-trigger was then used to induce the LLPS of ELP M80 within the lumen of the liposomes. By tuning the temperature of the system, a transition from a liquid phase (when the temperature of the sample was below the T_{cp},) to an aggregated structure (when heating the sample above the T_{cp} of the ELP) was observed.

Subsequently, a temperature ramp from 10 to 25 °C was applied to a sample of partially dewetted microdroplets encapsulating 1 mg.mL^{-1} ELP M80, as illustrated in Figure 2i. At 10 and 15°C, the solution inside the lumen of the vesicle was translucid and no organelles were formed (Figure 2i$_{1-2}$). As the temperature of the sample reached 19°C, slightly above the T_{cp} of the system,

the phase separation and assembly of the membraneless organelles slowly appeared (Figure 2i$_3$).

This phenomenon is intensified and finally completed at 25°C (Figure 2i$_4$, *See Supporting Information, Video S3*), denoted by the observation of the numerous black spots inside the liposomes under bright field. Furtherly, the reversibility of the process was investigated. As the sample was cooled below the T_{cp}, fewer organelles were present within the liposomes as ELPs returned to their liquid state (Figure 2i$_5$). Their complete disappearance, denoted by the lack observation of black spots in the artificial cytoplasm, was denoted at 10 °C (Figure 2i$_6$). Samples were subjected to 2 or 3 temperature cycles, and the phenomena observed were fully reversible with no hysteresis.
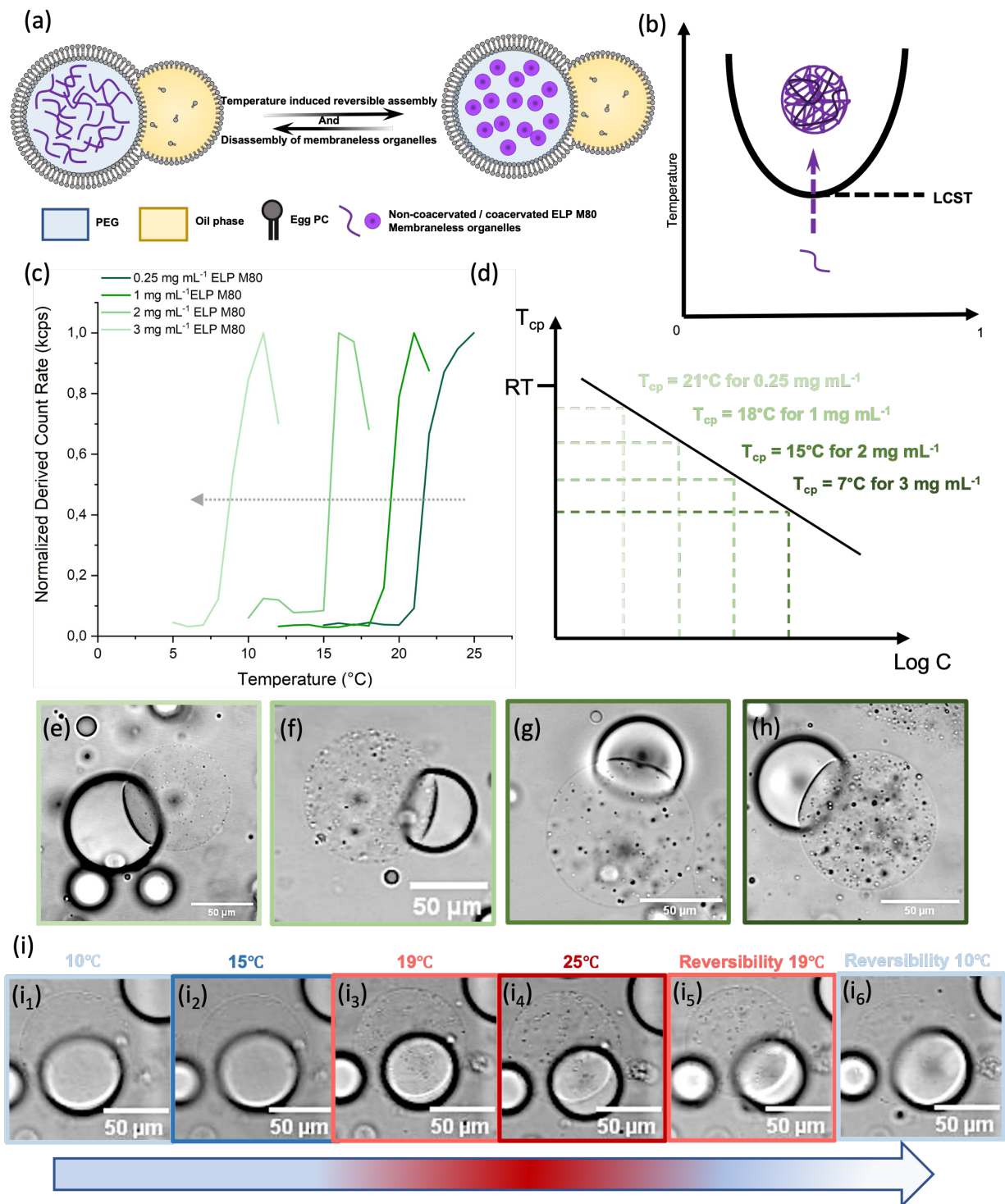
Figure 2. *Temperature-triggered assembly of synthetic organelles within partially dewetted liposomes (the oil reservoir appearing darker and more contrasted in the picture); a) Schematic illustration of ELP M80 synthetic membraneless organelles assembly inside cytomimetic lipid*

compartments in response to a temperature trigger; b) Schematic phase diagram of ELP phase separation; c) DLS analysis (measurement of the scattered light intensity, also referred to as the normalized derived count rate, DCR) to determine the T_{cp} of 0.25, 1, 2 and 3 mg.mL^{-1} of ELP M80 in a cell-like crowded environment; d) Schematic illustration of the T_{cp} evolution of ELP M80 as a function of concentration; e-h) Confocal images performed in bright field of partially dewetted liposomes encapsulating 0.25 mg.mL^{-1}, 1 mg.mL^{-1}, 2 mg.mL^{-1} and 3 mg.mL^{-1} of ELP M 80 respectively, in their phase separated state; i$_{1-6}$) Confocal images performed in bright field of partially dewetted liposomes encapsulating 1 mg.mL^{-1} ELP M80. A temperature ramp is exerted onto the sample from 10℃ to 25℃. The apparition of synthetic membraneless organelles is denoted by the appearance of black spots in the vesicles. A reverse temperature ramp is then applied from 25 to 10 ℃.

Synthetic membrane-bound organelles in partially dewetted vesicles.

Synthetic membrane-bound organelles were mimicked using PEG$_{22}$-*b*-PTMC$_{51}$-Cy5.5 vesicles, produced through a Dolomite™ microfluidic system. The organic solvent of samples collected at the output of microfluidic was removed by dialysis and vesicles were characterized by DLS. Table 1 presents a comparison between the hydrodynamic diameter and polydispersity index obtained using functionalized chains and those obtained from pure PEG$_{22}$-*b*-PTMC$_{51}$ vesicles, both produced under identical conditions that have previously demonstrated the homogenous formation of vesicles[72]. No drastic change was observed on vesicle size or polydispersity index when the fluorescently tagged-copolymer was incorporated. Consequently, the self-assembly of functionalized PEG$_{22}$-*b*-PTMC$_{51}$ vesicles tagged with cyanine 5.5 enables the formation of vesicles around 160 nm with a homogenous distribution.

Table 1: *Hydrodynamic diameter D_H and polydispersity index (PDI) acquisitions obtained by DLS 90° after self-assembly of PEG_{22}-b-$PTMC_{51}$ and PEG_{22}-b-$PTMC_{51}$-Cy5.5 vesicles. Purification performed by dialysis with a membrane tubing of 25 kDa cut-off, with 3 bath changes (of 2 L each) in 24 hrs.*

Sample	D_H (nm)	PDI
PEG_{22}-*b*-$PTMC_{51}$ without functionalization	161	0.138
PEG_{22}-*b*-$PTMC_{51}$ + 2 %wt Cy5.5 functionalized block copolymer	160	0.122

A concentration of 0.20 mg.mL^{-1} of these nanovesicles (calculated according to the concentration of block copolymers) was then dissolved in a PEG solution concentrated at 8 wt% and encapsulated within partially dewetted liposomes using the thick-shell microfluidic system described earlier (Figure 1). These systems were homogeneously spread within the liposomes, as observed by the appearance of fluorescence signal corresponding to the emitted fluorescence signal of cyanine 5.5 (Figure 3b and 3c). However, some vesicles seem larger than the size determined by DLS, probably due to some aggregation that might be induced by the PEG crowding that can act as a glue material or induce depletion forces.
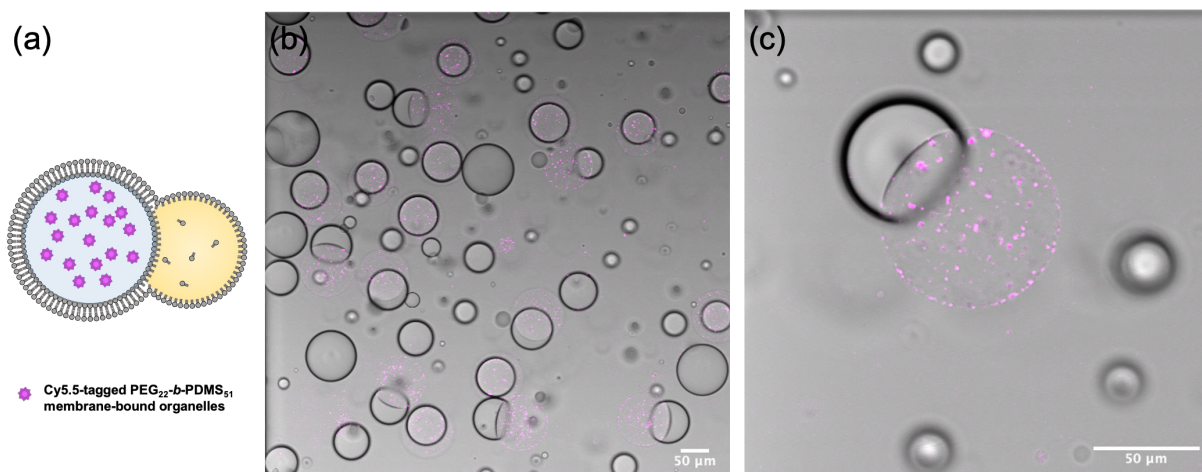
Figure 3. *Encapsulation of PEG22-b-PTMC5-Cy5.5 nanovesicles in partially dewetted microdroplets; (a) Scheme illustration of PEG22-b-PTMC51-Cy5.5 nanovesicles denoted by the fluorescent dots encapsulated in partially dewetted vesicles, corresponding to the fluorescence emission of cyanine 5.5; (b) Overview and (c) zoom of microdroplets embedding PEG22-b-PTMC51-Cy5.5 nanovesicles in a 8 wt% PEG solution. These images depict a superposition of images acquired under the bright field and the fluorescence mode (λExcitation/Emission = 633/650-730 nm).*

Co-encapsulation of membrane-bound and membraneless organelles.

The co-encapsulation of the two previous systems describing synthetic organelles within a same liposomal system was subsequently performed. 1 mg.mL^{-1} of ELP M80 was enclosed at the same time with 0.20 mg.mL^{-1} of PEG22-*b*-PTMC51-Cy5.5 nanovesicles, in a 8 wt% PEG solution. Temperature was used to trigger the phase-separation of ELP M80 and thus assemble the synthetic membraneless organelles (Figure 4a). A ramp temperature was performed from 10 to 25°C on the liposomal formulation (*See Supporting Information, Figure S1*). At 10 and 15°C, only the Cy5.5-tagged nanovesicles were observed within the liposomes (appearance of fluorescence signal), as the experiments were carried below the T_{cp} of the ELPs. Hence, no phase separation of the ELP

15

M80 occurred. (Figure 4b$_{1-2}$). As the experimental temperature was increased above the T_{cp} of the ELP M80, the assembly of membraneless organelles became evident, as marked by the emergence of dark black spots in the lumen under bright field acquisition (Figure 4b$_3$). This process continued until reaching full completion at 25°C (Figure 4b$_4$, *See Supporting Information, Video S4*). It is noteworthy to highlight that the membraneless organelles reverted to their liquid state, as the system was cooled down back to 10°C, leaving only the observation of nanovesicles that could freely move within partially dewetted liposomes (Figure 4b$_{5-6}$). Concerning the membrane-bound organelles, the nanovesicles exhibited a tendency to slightly sediment to the bottom of the liposomes, a phenomenon observed by multiple confocal image acquisitions that enabled us to have a representation of liposomes along the z-axis (*See Supporting Information, Figure S2*). Remarkably, the heating and cooling processes did not exert any discernible impact on the structural integrity of the nanovesicles.
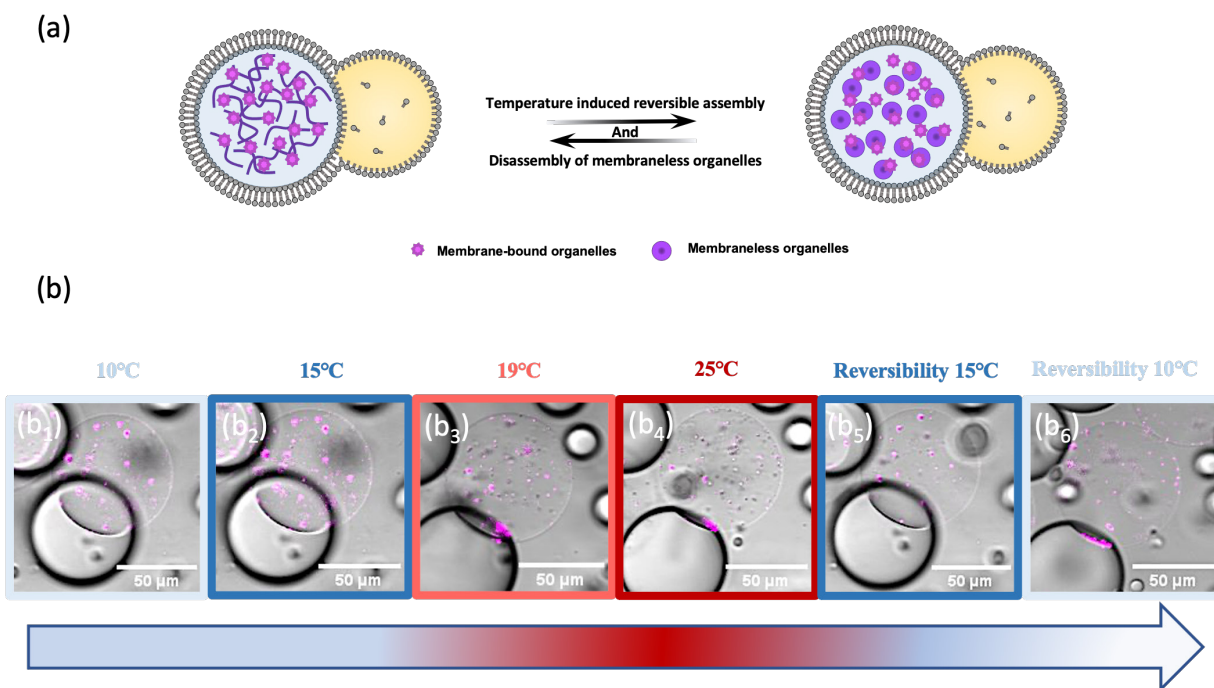
Figure 4. *Encapsulation of membrane-bound (PEG$_{22}$-b-PTMC$_{51}$-Cy5.5 nanovesicles) and membraneless (ELP M80) synthetic organelles; (a) Scheme illustration of vesicles encapsulating PEG$_{22}$-b-PTMC$_{51}$-Cy5.5 nanovesicles and ELP M80 before and after undergoing a phase separation as the T$_{cp}$ is reached; (b) Temperature ramp exerted on a sample of partially dewetted microdroplets. The presence of PEG$_{22}$-b-PTMC$_{51}$-Cy5.5 organelles with membrane is denoted by the pink dots (corresponding of the fluorescence signal of cyanine 5.5). The self-assembly and dismantling of ELP M80 membraneless organelles is denoted by the black dots. These images depict a superposition of images acquired under the bright field and the fluorescence mode ($\lambda_{Excitation}/_{Emission}$ = 633/650-730 nm).*

CONCLUSION

Our study successfully demonstrated the possibility of co-encapsulating different macromolecular components of eukaryotic cells through the utilization of specific microfluidic systems. At first, the formation of synthetic membraneless organelles within liposomes using a temperature-triggered assembly method and embedding temperature-sensitive elastin-like polypeptide (ELP M80) was performed. The cloud point temperatures were determined by varying the ELP concentrations to mimic cellular crowding. The concentration of 1 mg.mL^{-1} ELP M80 was identified as a suitable compromise for distinct membraneless organelle formation within liposomes. Temperature-triggered LLPS experiment demonstrated reversibility as cooling below the cloud point temperature caused the organelles to revert to a liquid state. Nanovesicles, were then encapsulated individually at first and their distribution within the partially dewetted liposomes

were homogenous, confirming by the uniform dispersion of fluorescence spots under confocal microscopy. When a co-encapsulation was performed with ELP M80, it was denoted that these two self-assembled systems can co-exist with minimal interaction, as the presence of membrane-bound nanoparticles did not hinder the LLPS and coacervation of ELP M80. Remarkably, the heating and cooling processes did not exert any discernible impact on the structural integrity of the nanovesicles or ELP M80 coacervates. This study provides insights into controlling the multi-component and multi-scale self-assembly of synthetic membraneless and membrane-bound organelles for potential applications in artificial cell models development. This breakthrough creates exciting opportunities for developing artificial cells from the bottom-up assembly and for exploring novel functions and interactions between these two types of organelles, similar to those that may occur inside living eukaryotic cells. The combination of such multi-component and multi-scale self-assembly properties, and the dynamic behavior of organelle formation do not only provide interesting models for biomimicry, but also may allow the design of functional bioreactors with tunable and activable response.

AUTHOR INFORMATION

Corresponding Author

* Corresponding Author: Sébastien Lecommandoux; Email : sebastien.lecommandoux@u-bordeaux.fr

Author Contributions

The manuscript was written through contributions of all authors. All authors have given approval to the final version of the manuscript.

Supporting Information

Additional confocal images, Z-stacks and videos highlighting the dynamic behavior of our system are available in the supporting information free of charge.

ABBREVIATIONS

LLPS Liquid-Liquid Phase Separation, ELP Elastin-Like Polypeptide, W/O/W water-in-oil-in-water emulsions, ATPS Aqueous Two-Phase System, IDP Intrinsically Disordered Protein, T_{cp} Cloud Point Temperature

REFERENCES

(1)   Szostak, J. W.; Bartel, D. P.; Luisi, P. L. Synthesizing Life. *Nature* **2001**, *409, 387-390*. https://doi.org/10.1038/35053176.

(2)   Marguet, M.; Bonduelle, C.; Lecommandoux, S. Multicompartmentalized Polymeric Systems: Towards Biomimetic Cellular Structure and Function. *Chem Soc Rev* **2013**, *42* (2), 512–529. https://doi.org/10.1039/C2CS35312A.

(3)   Roodbeen, R.; Van Hest, J. C. M. Synthetic Cells and Organelles: Compartmentalization Strategies. *BioEssays* **2009**, *31* (12), 1299–1308. https://doi.org/10.1002/bies.200900106.

(4)   Beales, P. A.; Ciani, B.; Mann, S. The Artificial Cell: Biology-Inspired Compartmentalization of Chemical Function. *Interface Focus* **2018**, *8* (5), 20180046. https://doi.org/10.1098/rsfs.2018.0046.

(5)   Guindani, C.; Da Silva, L. C.; Cao, S.; Ivanov, T.; Landfester, K. Synthetic Cells: From Simple Bio-Inspired Modules to Sophisticated Integrated Systems. *Angew. Chem. Int. Ed.* **2022**, *61* (16). https://doi.org/10.1002/anie.202110855.

(6)   Buddingh', B. C.; Van Hest, J. C. M. Artificial Cells: Synthetic Compartments with Life-like Functionality and Adaptivity. *Acc. Chem. Res.* **2017**, *50* (4), 769–777. https://doi.org/10.1021/acs.accounts.6b00512.

(7)   Peters, R. J. R. W.; Marguet, M.; Marais, S.; Fraaije, M. W.; van Hest, J. C. M.; Lecommandoux, S. Cascade Reactions in Multicompartmentalized Polymersomes. *Angew. Chem. Int. Ed.* **2014**, *53* (1), 146–150. https://doi.org/10.1002/anie.201308141.

(8)   Bolinger, P.-Y.; Stamou, D.; Vogel, H. Microfluidic Assembly of Monodisperse Vesosomes as Artificial Cell Models. *Angew. Chem. Int. Ed.* **2008**, *47* (30), 5544–5549. https://doi.org/10.1002/anie.200801606.

(9)   Peyret, A.; Ibarboure, E.; Pippa, N.; Lecommandoux, S. Liposomes in Polymersomes: Multicompartment System with Temperature-Triggered Release. *Langmuir* **2017**, *33* (28), 7079–7085. https://doi.org/10.1021/acs.langmuir.7b00655.

(10)   Mu, W.; Ji, Z.; Zhou, M.; Wu, J.; Lin, Y.; Qiao, Y. Membrane-Confined Liquid-Liquid Phase Separation toward Artificial Organelles. *Sci. Adv.* **2021**, *7* (22), eabf9000. https://doi.org/10.1126/sciadv.abf9000.

(11)   Moreau, N. G.; Martin, N.; Gobbo, P.; Tang, T.-Y. D.; Mann, S. Spontaneous Membrane-Less Multi-Compartmentalization via Aqueous Two-Phase Separation in Complex Coacervate Micro-Droplets. *Chem. Commun.* **2020**, *56* (84), 12717–12720. https://doi.org/10.1039/D0CC05399F.

(12)   Brangwynne, C. P.; Eckmann, C. R.; Courson, D. S.; Rybarska, A.; Hoege, C.; Gharakhani, J.; Jülicher, F.; Hyman, A. A. Germline P Granules Are Liquid Droplets That Localize by Controlled Dissolution/Condensation. *Science* **2009**, *324* (5935), 1729–1732. https://doi.org/10.1126/science.1172046.

(13)   Hyman, A. A.; Weber, C. A.; Jülicher, F. Liquid-Liquid Phase Separation in Biology. *Annu. Rev. Cell Dev. Biol.* **2014**, *30* (1), 39–58. https://doi.org/10.1146/annurev-cellbio-100913-013325.

(14)   Banani, S. F.; Lee, H. O.; Hyman, A. A.; Rosen, M. K. Biomolecular Condensates: Organizers of Cellular Biochemistry. *Nat. Rev. Mol. Cell Biol.* **2017**, *18* (5), 285–298. https://doi.org/10.1038/nrm.2017.7.

(15)   Bracha, D.; Walls, M. T.; Brangwynne, C. P. Probing and Engineering Liquid-Phase Organelles. *Nat. Biotechnol.* **2019**, *37* (12), 1435–1445. https://doi.org/10.1038/s41587-019-0341-6.

(16)   Chang, T. M. S. Semipermeable Microcapsules. *Science* **1964**, *146* (3643), 524–525.

https://doi.org/10.1126/science.146.3643.524.

(17)   Chang TMS. Hemoglobin corpuscles. Report of a research project for Honours Physiology, Medical Library, McGill University. Reprinted 1988 in J Biomaterials. *Artificial Cells & Artificial Organs.* **1957**, 16, 1-9.

(18)   Elani, Y.; Law, R. V.; Ces, O. Vesicle-Based Artificial Cells as Chemical Microreactors with Spatially Segregated Reaction Pathways. *Nat. Commun.* **2014**, *5* (1), 5305. https://doi.org/10.1038/ncomms6305.

(19)   Walde, P.; Cosentino, K.; Engel, H.; Stano, P. Giant Vesicles: Preparations and Applications. *ChemBioChem* **2010**, *11* (7), 848–865. https://doi.org/10.1002/cbic.201000010.

(20)   Weiss, M.; Frohnmayer, J. P.; Benk, L. T.; Haller, B.; Janiesch, J.-W.; Heitkamp, T.; Börsch, M.; Lira, R. B.; Dimova, R.; Lipowsky, R.; Bodenschatz, E.; Baret, J.-C.; Vidakovic-Koch, T.; Sundmacher, K.; Platzman, I.; Spatz, J. P. Sequential Bottom-up Assembly of Mechanically Stabilized Synthetic Cells by Microfluidics. *Nat. Mater.* **2018**, *17* (1), 89–96. https://doi.org/10.1038/nmat5005.

(21)   Zhu, T. F.; Szostak, J. W. Coupled Growth and Division of Model Protocell Membranes. *J. Am. Chem. Soc.* **2009**, *131* (15), 5705–5713. https://doi.org/10.1021/ja900919c.

(22)   Zong, W.; Ma, S.; Zhang, X.; Wang, X.; Li, Q.; Han, X. A Fissionable Artificial Eukaryote-like Cell Model. *J. Am. Chem. Soc.* **2017**, *139* (29), 9955–9960. https://doi.org/10.1021/jacs.7b04009.

(23)   Wang, X.; Tian, L.; Ren, Y.; Zhao, Z.; Du, H.; Zhang, Z.; Drinkwater, B. W.; Mann, S.; Han, X. Chemical Information Exchange in Organized Protocells and Natural Cell Assemblies with Controllable Spatial Positions. *Small* **2020**, *16* (27), 1906394. https://doi.org/10.1002/smll.201906394.

(24)   Wang, X.; Tian, L.; Du, H.; Li, M.; Mu, W.; Drinkwater, B. W.; Han, X.; Mann, S. Chemical Communication in Spatially Organized Protocell Colonies and Protocell/Living Cell Micro-Arrays. *Chem. Sci.* **2019**, *10* (41), 9446–9453. https://doi.org/10.1039/C9SC04522H.

(25)   Kurihara, K.; Okura, Y.; Matsuo, M.; Toyota, T.; Suzuki, K.; Sugawara, T. A Recursive Vesicle-Based Model Protocell with a Primitive Model Cell Cycle. *Nat. Commun.* **2015**, *6* (1), 8352. https://doi.org/10.1038/ncomms9352.

(26)   Che, H.; Cao, S.; van Hest, J. C. M. Feedback-Induced Temporal Control of "Breathing" Polymersomes To Create Self-Adaptive Nanoreactors. *J. Am. Chem. Soc.* **2018**, *140* (16), 5356–5359. https://doi.org/10.1021/jacs.8b02387.

(27)   Kamat, N. P.; Katz, J. S.; Hammer, D. A. Engineering Polymersome Protocells. *J. Phys. Chem. Lett.* **2011**, *2* (13), 1612–1623. https://doi.org/10.1021/jz200640x.

(28)   Jiang, W.; Zhou, Y.; Yan, D. Hyperbranched Polymer Vesicles: From Self-Assembly, Characterization, Mechanisms, and Properties to Applications. *Chem. Soc. Rev.* **2015**, *44* (12), 3874–3889. https://doi.org/10.1039/C4CS00274A.

(29)   LoPresti, C.; Lomas, H.; Massignani, M.; Smart, T.; Battaglia, G. Polymersomes: Nature Inspired Nanometer Sized Compartments. *J. Mater. Chem.* **2009**, *19* (22), 3576. https://doi.org/10.1039/b818869f.

(30)   Rikken, R. S. M.; Engelkamp, H.; Nolte, R. J. M.; Maan, J. C.; van Hest, J. C. M.; Wilson, D. A.; Christianen, P. C. M. Shaping Polymersomes into Predictable Morphologies via Out-of-Equilibrium Self-Assembly. *Nat. Commun.* **2016**, *7* (1), 12606. https://doi.org/10.1038/ncomms12606.

(31)   Matoori, S.; Leroux, J.-C. Twenty-Five Years of Polymersomes: Lost in Translation? *Mater. Horiz.* **2020**, *7* (5), 1297–1309. https://doi.org/10.1039/C9MH01669D.

(32)   Huang, X.; Li, M.; Green, D. C.; Williams, D. S.; Patil, A. J.; Mann, S. Interfacial Assembly of Protein–Polymer Nano-Conjugates into Stimulus-Responsive Biomimetic Protocells. *Nat. Commun.* **2013**, *4* (1), 2239. https://doi.org/10.1038/ncomms3239.

(33)   Huang, X.; Patil, A. J.; Li, M.; Mann, S. Design and Construction of Higher-Order Structure and Function in Proteinosome-Based Protocells. *J. Am. Chem. Soc.* **2014**, *136* (25), 9225–9234. https://doi.org/10.1021/ja504213m.

(34)   Li, M.; Harbron, R. L.; Weaver, J. V. M.; Binks, B. P.; Mann, S. Electrostatically Gated Membrane Permeability in Inorganic Protocells. *Nat. Chem.* **2013**, *5* (6), 529–536. https://doi.org/10.1038/nchem.1644.

(35)   Tian, L.; Martin, N.; Bassindale, P. G.; Patil, A. J.; Li, M.; Barnes, A.; Drinkwater, B. W.; Mann, S. Spontaneous Assembly of Chemically Encoded Two-Dimensional Coacervate Droplet Arrays by Acoustic Wave Patterning. *Nat. Commun.* **2016**, *7* (1), 13068. https://doi.org/10.1038/ncomms13068.

(36)   Koga, S.; Williams, D. S.; Perriman, A. W.; Mann, S. Peptide–Nucleotide Microdroplets as a Step towards a Membrane-Free Protocell Model. *Nat. Chem.* **2011**, *3* (9), 720–724. https://doi.org/10.1038/nchem.1110.

(37)   Aumiller, W. M.; Keating, C. D. Phosphorylation-Mediated RNA/Peptide Complex Coacervation as a Model for Intracellular Liquid Organelles. *Nat. Chem.* **2016**, *8* (2), 129–137. https://doi.org/10.1038/nchem.2414.

(38)   Deng, N.; Huck, W. T. S. Microfluidic Formation of Monodisperse Coacervate Organelles in Liposomes. *Angew. Chem. Int. Ed.* **2017**, *56* (33), 9736–9740. https://doi.org/10.1002/anie.201703145.

(39)   Belluati, A.; Thamboo, S.; Najer, A.; Maffeis, V.; Planta, C.; Craciun, I.; Palivan, C. G.; Meier, W. Multicompartment Polymer Vesicles with Artificial Organelles for Signal-Triggered Cascade Reactions Including Cytoskeleton Formation. *Adv. Funct. Mater.* **2020**, *30* (32), 2002949. https://doi.org/10.1002/adfm.202002949.

(40)   Hindley, J. W.; Zheleva, D. G.; Elani, Y.; Charalambous, K.; Barter, L. M. C.; Booth, P. J.; Bevan, C. L.; Law, R. V.; Ces, O. Building a Synthetic Mechanosensitive Signaling Pathway in Compartmentalized Artificial Cells. *Proc. Natl. Acad. Sci.* **2019**, *116* (34), 16711–16716. https://doi.org/10.1073/pnas.1903500116.

(41)   Deng, N.-N.; Yelleswarapu, M.; Zheng, L.; Huck, W. T. S. Microfluidic Assembly of Monodisperse Vesosomes as Artificial Cell Models. *J. Am. Chem. Soc.* **2017**, *139* (2), 587–590. https://doi.org/10.1021/jacs.6b10977.

(42)   Boyer, C.; Zasadzinski, J. A. Multiple Lipid Compartments Slow Vesicle Contents Release in Lipases and Serum. *ACS Nano* **2007**, *1* (3), 176–182. https://doi.org/10.1021/nn7002025.

(43)   Li, S.; Wang, X.; Mu, W.; Han, X. Chemical Signal Communication between Two Protoorganelles in a Lipid-Based Artificial Cell. *Anal. Chem.* **2019**, *91* (10), 6859–6864. https://doi.org/10.1021/acs.analchem.9b01128.

(44)   Hindley, J. W.; Elani, Y.; McGilvery, C. M.; Ali, S.; Bevan, C. L.; Law, R. V.; Ces, O. Light-Triggered Enzymatic Reactions in Nested Vesicle Reactors. *Nat. Commun.* **2018**, *9* (1), 1093. https://doi.org/10.1038/s41467-018-03491-7.

(45)   Kreft, O.; Prevot, M.; Möhwald, H.; Sukhorukov, G. B. Shell-in-Shell Microcapsules: A Novel Tool for Integrated, Spatially Confined Enzymatic Reactions. *Angew. Chem. Int. Ed.* **2007**, *46* (29), 5605–5608. https://doi.org/10.1002/anie.200701173.

(46)   Marguet, M.; Edembe, L.; Lecommandoux, S. Polymersomes in Polymersomes: Multiple

Loading and Permeability Control. *Angew. Chem.* **2012**, *124* (5), 1199–1202. https://doi.org/10.1002/ange.201106410.

(47)   Städler, B.; Chandrawati, R.; Goldie, K.; Caruso, F. Capsosomes: Subcompartmentalizing Polyelectrolyte Capsules Using Liposomes. *Langmuir* **2009**, *25* (12), 6725–6732. https://doi.org/10.1021/la900213a.

(48)   Huang, X.; Voit, B. Progress on Multi-Compartment Polymeric Capsules. *Polym Chem* **2013**, *4* (3), 435–443. https://doi.org/10.1039/C2PY20636F.

(49)   Maina, J. W.; Richardson, J. J.; Chandrawati, R.; Kempe, K.; Van Koeverden, M. P.; Caruso, F. Capsosomes as Long-Term Delivery Vehicles for Protein Therapeutics. *Langmuir* **2015**, *31* (28), 7776–7781. https://doi.org/10.1021/acs.langmuir.5b01667.

(50)   Garenne, D.; Beven, L.; Navailles, L.; Nallet, F.; Dufourc, E. J.; Douliez, J.-P. Sequestration of Proteins by Fatty Acid Coacervates for Their Encapsulation within Vesicles. *Angew. Chem.* **2016**, *128* (43), 13673–13677. https://doi.org/10.1002/ange.201607117.

(51)   Love, C.; Steinkühler, J.; Gonzales, D. T.; Yandrapalli, N.; Robinson, T.; Dimova, R.; Tang, T. -Y. D. Reversible pH-Responsive Coacervate Formation in Lipid Vesicles Activates Dormant Enzymatic Reactions. *Angew. Chem.* **2020**, *132* (15), 6006–6013. https://doi.org/10.1002/ange.201914893.

(52)   Deshpande, S.; Brandenburg, F.; Lau, A.; Last, M. G. F.; Spoelstra, W. K.; Reese, L.; Wunnava, S.; Dogterom, M.; Dekker, C. Spatiotemporal Control of Coacervate Formation within Liposomes. *Nat. Commun.* **2019**, *10* (1), 1800. https://doi.org/10.1038/s41467-019-09855-x.

(53)   Last, M. G. F.; Deshpande, S.; Dekker, C. pH-Controlled Coacervate–Membrane Interactions within Liposomes. *ACS Nano* **2020**, *14* (4), 4487–4498. https://doi.org/10.1021/acsnano.9b10167.

(54)   Kojima, T.; Takayama, S. Membraneless Compartmentalization Facilitates Enzymatic Cascade Reactions and Reduces Substrate Inhibition. *ACS Appl. Mater. Interfaces* **2018**, *10* (38), 32782–32791. https://doi.org/10.1021/acsami.8b07573.

(55)   Li, J.; Xu, Z.; Zhu, M.; Zhao, C.; Wang, X.; Chen, H.; Liu, X.; Wang, L.; Huang, X. Programmable Spatial Organization of Liquid-Phase Condensations. *Chem* **2022**, *8* (3), 784–800. https://doi.org/10.1016/j.chempr.2021.11.011.

(56)   Zhao, H.; Ibarboure, E.; Ibrahimova, V.; Xiao, Y.; Garanger, E.; Lecommandoux, S. Spatiotemporal Dynamic Assembly/Disassembly of Organelle-Mimics Based on Intrinsically Disordered Protein-Polymer Conjugates. *Adv. Sci.* **2021**, *8* (24), 2102508. https://doi.org/10.1002/advs.202102508.

(57)   Zhao, H.; Ibrahimova, V.; Garanger, E.; Lecommandoux, S. Dynamic Spatial Formation and Distribution of Intrinsically Disordered Protein Droplets in Macromolecularly Crowded Protocells. *Angew. Chem. Int. Ed.* **2020**, *59* (27), 11028–11036. https://doi.org/10.1002/anie.202001868.

(58)   Booth, R.; Qiao, Y.; Li, M.; Mann, S. Spatial Positioning and Chemical Coupling in Coacervate-in-Proteinosome Protocells. *Angew. Chem. Int. Ed.* **2019**, *58* (27), 9120–9124. https://doi.org/10.1002/anie.201903756.

(59)   Zhao, Q.; Cao, F.; Luo, Z.; Huck, W. T. S.; Deng, N. Photoswitchable Molecular Communication between Programmable DNA-Based Artificial Membraneless Organelles. *Angew. Chem. Int. Ed.* **2022**, *61* (14). https://doi.org/10.1002/anie.202117500.

(60)   Chen, Y.; Yuan, M.; Zhang, Y.; Liu, S.; Yang, X.; Wang, K.; Liu, J. Construction of Coacervate-in-Coacervate Multi-Compartment Protocells for Spatial Organization of Enzymatic Reactions. *Chem. Sci.* **2020**, *11* (32), 8617–8625. https://doi.org/10.1039/D0SC03849K.

(61)   Wang, C.; Yang, J.; Lu, Y. Modularize and Unite: Toward Creating a Functional Artificial Cell. *Front. Mol. Biosci.* **2021**, *8*, 781986. https://doi.org/10.3389/fmolb.2021.781986.

(62)   Schvartzman, C.; Zhao, H.; Ibarboure, E.; Ibrahimova, V.; Garanger, E.; Lecommandoux, S. Control of Enzyme Reactivity in Response to Osmotic Pressure Modulation Mimicking Dynamic Assembly of Intracellular Organelles. *Adv. Mater.* **2023**, *35* (33), 2301856. https://doi.org/10.1002/adma.202301856.

(63)   Chang, M.-Y.; Ariyama, H.; Huck, W. T. S.; Deng, N.-N. Division in Synthetic Cells. *Chem. Soc. Rev.* **2023**, *52*, 3307-3325. https://doi.org/10.1039/D2CS00985D.

(64)   Wang, X.; Wu, S.; Tang, T.-Y. D.; Tian, L. Engineering Strategies for Sustainable Synthetic Cells. *Trends Chem.* **2022**, *4* (12), 1106–1120. https://doi.org/10.1016/j.trechm.2022.09.011.

(65)   Zhao, Y. G.; Zhang, H. Phase Separation in Membrane Biology: The Interplay between Membrane-Bound Organelles and Membraneless Condensates. *Dev. Cell* **2020**, *55* (1), 30–44. https://doi.org/10.1016/j.devcel.2020.06.033.

(66)   Meyer, D. E.; Chilkoti, A. Purification of Recombinant Proteins by Fusion with Thermally-Responsive Polypeptides. *Nat. Biotechnol.* **1999**, *17* (11), 1112–1115. https://doi.org/10.1038/15100.

(67)   Petitdemange, R.; Garanger, E.; Bataille, L.; Bathany, K.; Garbay, B.; Deming, T. J.; Lecommandoux, S. Tuning Thermoresponsive Properties of Cationic Elastin-like Polypeptides by Varying Counterions and Side-Chains. *Biomacromolecules* **2017**, *18*, 544.

(68)   Petitdemange, R. Chemoselective Modifications of Recombinant Elastin-like Polypeptides: Tuning Thermosensitivity and Bioactivity, Bordeaux, 2016. https://theses.hal.science/tel-01552303v2.

(69)   Kramer, J. R.; Petitdemange, R.; Bataille, L.; Bathany, K.; Wirotius, A.-L.; Garbay, B.; Deming, T. J.; Garanger, E.; Lecommandoux, S. Quantitative Side-Chain Modifications of Methionine-Containing Elastin-Like Polypeptides as a Versatile Tool to Tune Their Properties. *ACS Macro Lett.* **2015**, *4* (11), 1283–1286. https://doi.org/10.1021/acsmacrolett.5b00651.

(70)   Urry, D. W. Physical Chemistry of Biological Free Energy Transduction As Demonstrated by Elastic Protein-Based Polymers. *J. Phys. Chem. B* **1997**, *101* (51), 11007–11028. https://doi.org/10.1021/jp972167t.

(71)   Keating, C. D. Aqueous Phase Separation as a Possible Route to Compartmentalization of Biological Molecules. *Acc. Chem. Res.* **2012**, *45* (12), 2114–2124. https://doi.org/10.1021/ar200294y.

(72)   Martin, A.; Lalanne, P.; Weber-Vax, A.; Mutschler, A.; Lecommandoux, S. Controlling Polymersome Size through Microfluidic-Assisted Self-Assembly: Enabling 'Ready to Use' Formulations for Biological Applications. *Int. J. Pharm.* **2023**, *642*, 123157. https://doi.org/10.1016/j.ijpharm.2023.123157.
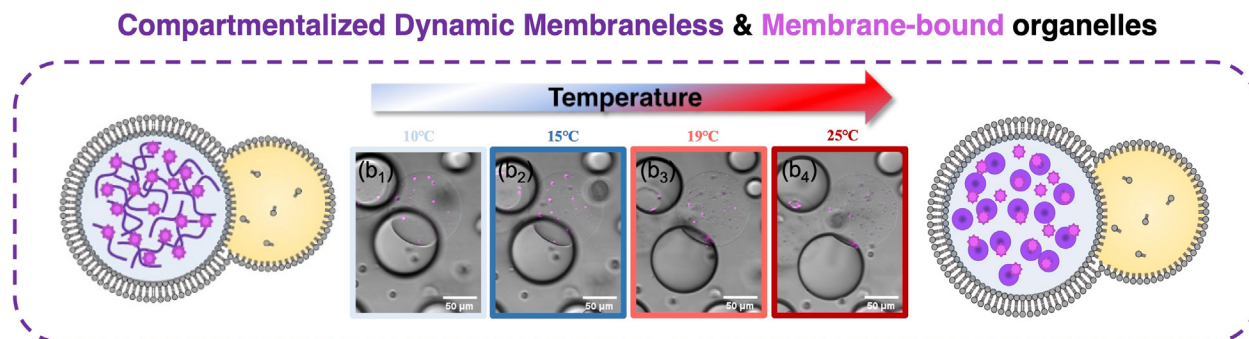
Figure for TOC

Protocells Featuring Membrane-Bound and Dynamic Membraneless Organelles

Clémence Schvartzman, Emmanuel Ibarboure, Anouk Martin, Elisabeth Garanger, Angela

Mutschler, Sébastien Lecommandoux*

Univ. Bordeaux, CNRS, Bordeaux INP, LCPO, UMR 5629, F-33600 Pessac, France
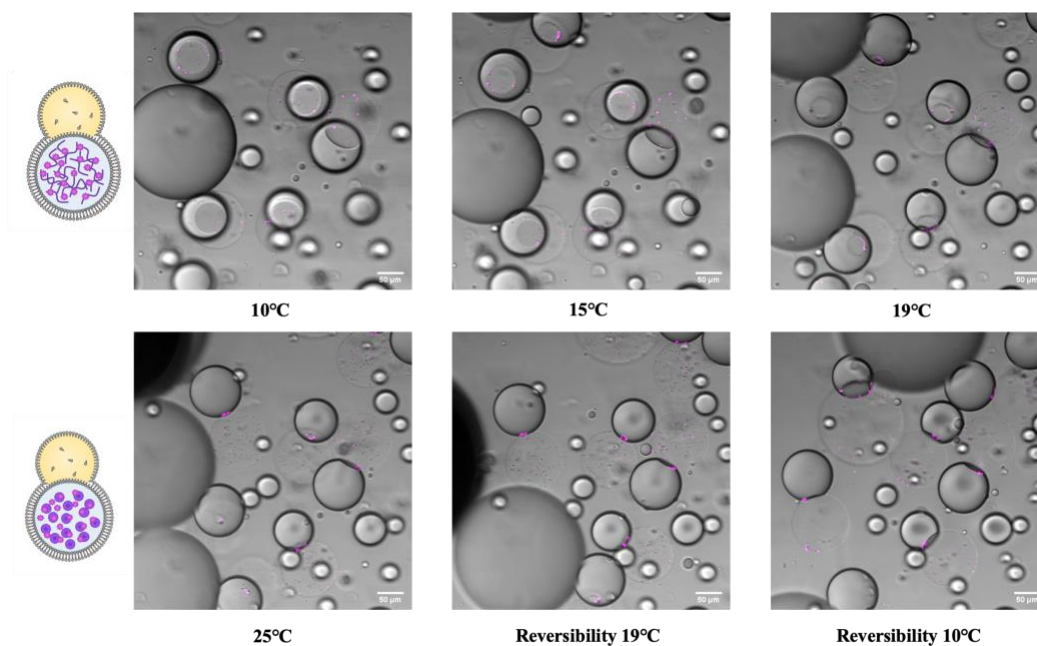
Figure S1. *Overview of the sample where Figure 5b$_{1-6}$ was extracted from. Plate heater was set at 25 °C. These images depict a superposition of images acquired under bright field and fluorescence excitation and emission at 633/730 nm.*
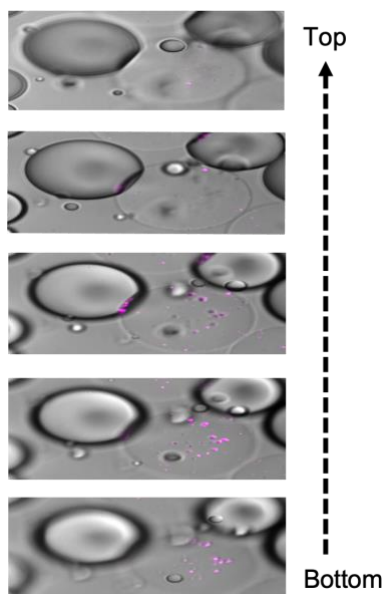
Figure S2. *Bottom-up view of the inside of a partially dewetted liposome, where it can be observed that the Cy5.5-tagged nanovesicles dropped to the bottom of the vesicle. These images depict a superposition of images acquired under the bright field and the fluorescence mode (excitation and emission at 633/730 nm).*

Video S3. *Video of synthetic membraneless organelles assembled within partially dewetted microdroplets taken under confocal microscope in the bright field mode. Plate heater was set at 25°C.*

Video S4. *Video of PEG$_{22}$-b-PTMC$_{51}$-Cy5.5 nanovesicles encapsulated with phase separated ELP M80 inside of partially dewetted vesicles. Video was taken at 25°C under the bright field mode.*